Journal of Power Sources 195 (2010) 3849–3857

Contents lists available at ScienceDirect

Journal of Power Sources

journal homepage: www.elsevier.com/locate/jpowsour

A flexible direct methanol micro-fuel cell based on a metalized, photosensitive polymer film

C. Weinmueller, G. Tautschnig, N. Hotz, D. Poulikakos*

Laboratory of Thermodynamics in Emerging Technologies, Institute of Energy Technology, Department of Mechanical and Process Engineering, ETH Zürich, 8092 Zürich, Switzerland

ARTICLE INFO

Article history:
Received 14 August 2009
Received in revised form
27 November 2009
Accepted 20 December 2009
Available online 11 January 2010

Keywords:
Direct methanol micro-fuel cell
Portable power
Flexible fuel cell
Polymer-based fuel cell
SU-8 fuel cell
Thin-film fuel cell

ABSTRACT

This paper presents and investigates a concept for a flexible direct methanol micro-fuel cell (FDMMFC) based on the microstructuring of a Cr/Au metalized, thin polymer film of photosensitive SU-8. The inscribed microchannels in the electrodes are 200 μm × 200 μm in crosssection and spanning an active fuel cell area of 10 mm × 10 mm with a Pt-black catalyst on the cathode side of the membrane electrode assembly (MEA) and a Pt–Ru alloy catalyst on the anode side. Subsequently, the paper focuses on a thorough electrical characterization of the FDMMFC, under the employment of a variable resistor simulating an electrical load as well as a classical galvanostatical measurement technique. The fuel cell is also tested while operating in a bent, non-flat configuration. An extensive parameter study revealed an optimal and long-term stable operating condition for the fuel cell employing for both electrodes a serpentine flow field and a volume flow rate of 0.14 ml min^{-1} of a 1 M methanol solution at the anode side with a gas volume flow rate of 8 ml min^{-1} of humidified O_2 at the cathode side yielding a power density of 19.0 mW cm^2 at 75 mA cm^2 at a temperature of 60 °C.

Furthermore, a flow-visualization of the two-phase flow occurring at the anode side has been performed by utilizing fluorescence microscopy. The strong influence of the two-phase flow on the performance of a fuel cell at high current densities becomes apparent in correlating the observed flow patterns with the corresponding current density of the polarization curve. The paper also investigates the functionality of the present FDMMFC under different bent conditions. The tests showed an insignificant drop of the electrical performance under bending due to an inhomogeneous contact resistance.

1. Introduction

The tremendous increase in the power demand of mobile electronics, such as cell phones, iPods® or personal digital assistances (PDA), has outbalanced the parallel development of higher energy density Li-ion batteries creating a "power-gap" scenario [1]. The constant size-reduction of integrated circuit (IC) technology approximately following Moore's law [2] allows an ever-increasing number and density of functionality on electronic devices, respectively. On the other hand, the Li-ion battery has not kept pace with the today's power requirements of portable electronic devices [3,4].

The miniaturization of fuel cells due to the application of standardized fabrication techniques classically used in microelectromechnical systems (MEMS) and the direct integration into portable and mobile applications bears an enormous potential for the battery substitution as many recent publications indicate [1,5–11].

Kelley et al. [12] devised the first silicon-based rigid micro-direct methanol fuel cell (DMFC) adapted from the fabrication process of Kovacs et al. [13]. The hot pressed assembly yielded a maximum power density of 60 mW cm^{-2} at 300 mA cm^{-2} at a temperature of 70 °C by employing a Nafion®-117 membrane with a spray-coated Pt-black Nafion® solution at the cathode side (Pt loading: 2.5 mg cm^{-2}) and electrodeposited Pt–Ru carbon on the anode side (Pt–Ru loading: 4.0 mg cm^{-2}).

Lu et al. [7] presented a parameter study of a silicon-based, Cr/Cu/Au-coated rigid micro-DMFC with a novel membrane electrode assembly (MEA), which reduces methanol crossover. The gas diffusion layer on the anode side is coated with a mixture of carbon black and Teflon® increasing the diffusion resistance of methanol to the electrolyte. They report a maximum power output of 50 mW cm^{-2} at 200 mA cm^{-2} for a 2 M methanol fed micro-DMFC at 60 °C; the catalyst loading for the anode is 4–6 mg cm^{-2} Pt–Ru and for the cathode is 1.3 mg cm^{-2} Pt.

Cha et al. [9] reported as one of the first of an all-polymer micro-DMFC fabricated of a UV-sensitive photoresist structured by standard IC fabrication techniques. The all-polymer bipolar plate with an array of through-holes structures the sandwiched

* Corresponding author. Tel.: +41 44 632 2435; fax: +41 44 632 1176.
E-mail address: dimos.poulikakos@ethz.ch (D. Poulikakos).

0378-7753/$ – see front matter © 2010 Elsevier B.V. All rights reserved.
doi:10.1016/j.jpowsour.2009.12.092

Nafion-115 membrane in single, parallel operating fuel cells with no fluid channels being inscribed in the electrode achieving a maximum power density of 8 mW cm^{-2} at a current density of 37 mA cm^{-2}.

In the design and fabrication study of Park and Madou [1] a micro-scale pyrolyzed carbon fluidic plate of a miniaturized polymer electrolyte membrane fuel cell (PEMFC) is presented as an alternative to standard MEMS materials such as silicon, glass, ceramics and photoresists. The assembled micro-PEMFC cell with a Nafion®-115 MEA yielded in the proof-of-concept experiment a maximum power output of 1.21 mW cm^{-2}.

Nevertheless, the rigid substrate, silicon, limits the application of micro-fuel cells to present microelectronic sensors and devices. Therefore, new electrode materials and adapted fabrication processes have to be considered to meet future needs of electronics applications. Cutting-edge research activities [14–16] show that future electronic devices are going to extend the requirements for mobile applications to flexible substrates introducing functionalized polymers as base materials.

This study presents and electrically characterizes a concept of a flexible direct methanol micro-fuel cell (FDMMFC) to meet the requirements of a flexible and portable high power density unit. The fuel cell electrodes are devised of thin polymer films structured by adapted, but nevertheless standard microfabrication techniques generally employed for MEMS. The evident advantage is the easy scale-up of the process to industrial scales and levels. The material of choice is SU-8, a photosensitive and very firm epoxy, commonly known in MEMS processes as a photoresist easily being structured by photolithography. The challenge of the electrode fabrication, similar to general flexible electronics, is the functionalized metallization of the dielectric base substance, the polymer. During the course of the paper, we show that a physical vapour deposition of a Cr/Au bilayer will perfectly serve as a conductor even under severe bending and different temperature levels.

Further, we investigate the electrical performance of the newly devised bendable fuel cell assembly (FCA) with two techniques, with a variable resistor and galvanostatically, under the influence of volume flow rates and temperature levels in two different classical flow field designs, a parallel and a serpentine flow field. The study is concluded with a visualization of the occurring two-phase flow in the anode flow field and its correlation to the corresponding current density.

2. Experimental

2.1. Microfabrication

A combination of standard microfabrication/MEMS techniques [17] with secondary modifications based on photolithography was applied to manufacture micro-sized flow fields in silicon and SU-8 films, see fabrication steps in Fig. 1. The electrodes are designed with an active area of 10 mm × 10 mm and include an inscribed microchannel network of 200 μm depth and width; the separating rib structure is 200 μm wide. Two different flow fields, serpentine and parallel, have been investigated as seen in Fig. 2.

2.1.1. SU-8-based bipolar plates

A 500 ± 25 μm thick, p-doped, single-side polished, 4" silicon wafer used as a substrate is spin-coated with a 2.5 μm sacrificial layer (LOR 30B, MicroChem Corp.) and soft baked at 200 °C to evaporate any solvent. Subsequently, the SU-8 layer (SU-8 100, MicroChem Corp.) is applied with a thickness of 210 ± 20 μm with the following parameters: 30 s at 500 rpm (200 rpm s^{-1} acceleration) and 30 s at 1300 rpm (300 rpm s^{-1} acceleration). After a resting period of 30 min at ambient room conditions a soft bake is performed by incrementally altering the temperature of a hot plate from 65 °C (for 25 min) to 95 °C (for 70 min) to 65 °C (for 5 min) to room temperature (for 10 min) with a temperature ramping of 35%.

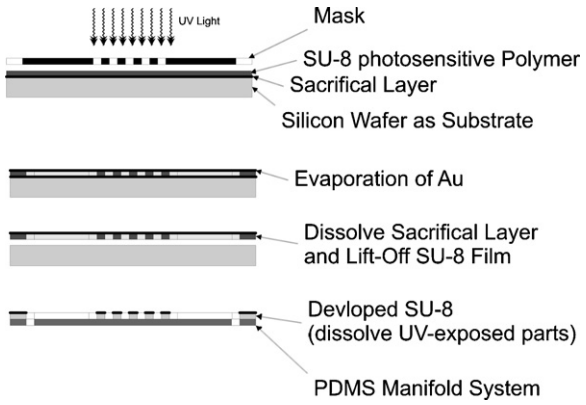

Fig. 1. Process flow for the fabrication of the SU-8 based electrode: application of a sacrificial layer and a SU-8 layer, photolithography, metallization with Cr and Au, lift-off of SU-8 electrode, development and removal of unexposed parts and attachment to PDMS manifold.

In the subsequent photolithographic process step (MA6, Süss Micro Tec), the mask polarity of a deployed UV-transparent foil mask (dpi ≥2400, check) patterns the photoresist during the UV exposure with a dose of 700 mJ cm^{-2}.

Before postbaking (1 h @ STP; 5 min @ 65 °C; 30 min @ 95 °C; 5 min @ 75 °C; 5 min @ 65 °C; 15 min @ STP and a ramping rate 35%) and developing (SU-8 Developer, MicroChem Corp.) the SU-8 layer, the surface is metalized by a E-Beam PVD technique (E-Beam PVD, Edwards E306) depositing 20 nm Cr and 200 nm Au, respectively. Consecutively, the metal-coated SU-8 film is removed from the substrate by a lift-off bath for 15 min (PG Remover, MicroChem Corp.). The SU-8 electrodes are immersed in a distilled deionized ultrasonic water bath, in order to rapture the Cr/Au-diaphragm still bridging the microchannels and simultaneously cleaning the surface of the SU-8 bipolar plates from remains of developer and remover, respectively.

2.1.2. Manifold microchannels in PDMS

The fluids are distributed in a manifold incorporated as microchannels in a polydimethylsiloxane block (PDMS), see Fig. 3, and fabricated according to standard soft-lithography techniques [17,18]. The negative form of the microchannel structure is manufactured in analogy to the above mentioned procedure, however, without a sacrificial layer between the substrate and the SU-8 structures to serve as a mold. The unconcealed surface is passivated by exposing the mold to silane vapor (tridecafluoro-1,1,22-tetrahydrooctyl-1-1trichlorosilane; United Chemical Technologies, Bristol, PA) for 2 h. The PDMS oligomer is premixed with the crosslinking agent (Sylgard 184, Dow Corning, Midland, MI) at the

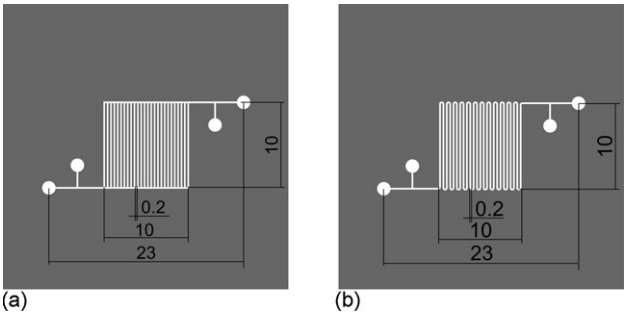

Fig. 2. Schematic of the ICP inscribed flow field into the electrode: (a) parallel and (b) serpentine.

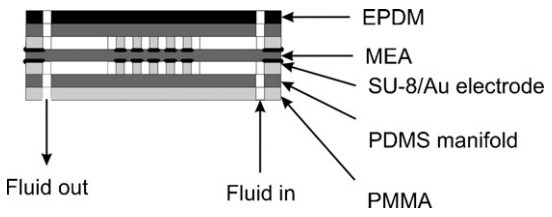

Fig. 3. Schematic of the fuel cell assembly without the outer holder and heating block.

ratio of 1:10 wt%, cast on the mold and degassed under low vacuum conditions for 30 min. The subsequent crosslinking process is activated in a convection oven at 65 °C for 1 h. The PDMS form with the incorporated microchannels is lifted off and diced in the according pieces.

2.2. Fuel cell preparation and assembly

2.2.1. MEA preparation

The membrane electrode assembly (MEA, Lynntech Inc., Texas), the heart of a polymer fuel cell, consists of a Nafion®-117 membrane coated 10 mm × 10 mm on the anode side with a Pt–Ru catalyst (Pt–Ru loading: 4 mg cm^{-2}) and on the cathode side with Pt-black (Pt loading: 4 mg cm^{-2}) forming the active area of the fuel cell.

Prior to the assembling of the MEA, it is rinsed with and thereafter immersed in deionized, distilled water (Millipore, resistivity: 15 MΩ) for 24 h. It has been refrained from employing a performance enhancing pretreatment of the MEA as described in [7,9], since the referred-to procedure saturates the MEA with H^+ ions leading as a consequence to a short-term performance boosting behavior. The long-term immersion of the MEA in distilled and highly deionized water is efficiently removing a high quantity of unwanted ions inside the MEA.

Due to the deleterious effect of cathode flooding in a parallel flow field at the cathode side (tested, but not shown here), only serpentine structured cathode flow fields are employed throughout the following parameter study.

2.2.2. Micro-fuel cell assembly

The micro-DMFC was assembled inside the upper stainless steel holder by aligning the sealing sheet (EPDM, Aspag AG), the PDMS manifold, the cathode side SU-8 electrode, the pretreated MEA, the anode side SU-8 electrode, the PDMS manifold, a stabilizing PMMA plate (Plexiglas®) and finally the lower stainless steel holder as illustrated in the schematic, Fig. 3. An aluminum heating block with a maximum power output of 10 W was placed around the assembly and tightened with 12 equally spaced screws to the upper holder in order to apply a homogenous contact pressure within the fuel cell assembly and, furthermore, to provide a constant contact resistance across the electrodes.

The transparency of the PMMA plate and of the PDMS manifold allow for optical access to the microchannels of the anode side flow field. The upper and lower stainless steel holders provide an integrated fluid supply manifold and pressure ports to the electrodes.

The electrical circuit is completed by inserting/sandwiching a partially insulated film-electrode between the bipolar plate and the MEA. Finally, a continuity test ensures two electrically isolated electrodes.

2.3. Test apparatus and procedure

2.3.1. Experimental setup

The experiments were performed under standard laboratory conditions, 22 °C and 100 kPa ambient, in the experimental apparatus shown in Fig. 4. A syringe pump (Harvard Apparatus, PHD4400 programmable) delivers the desired fluid flow V_l of the aqueous methanol solution ranging from 0.035 to 0.56 ml min^{-1}. A 1 M methanol solution was chosen throughout the experimental series as the optimal methanol concentration according to literature [19,20]. Three differential pressure sensors (Huba Control 692; 0.2, 2.5, 25 bar) have been employed to record the pressure drop across the microchannel network of the flow fields.

On the cathode side, the precise gas composition is supplied by pressurized gas cylinders of N_2 (PanGas, purity ≥99.995%) and O_2 (PanGas, purity ≥99.95%) and is adjusted by two mass flow

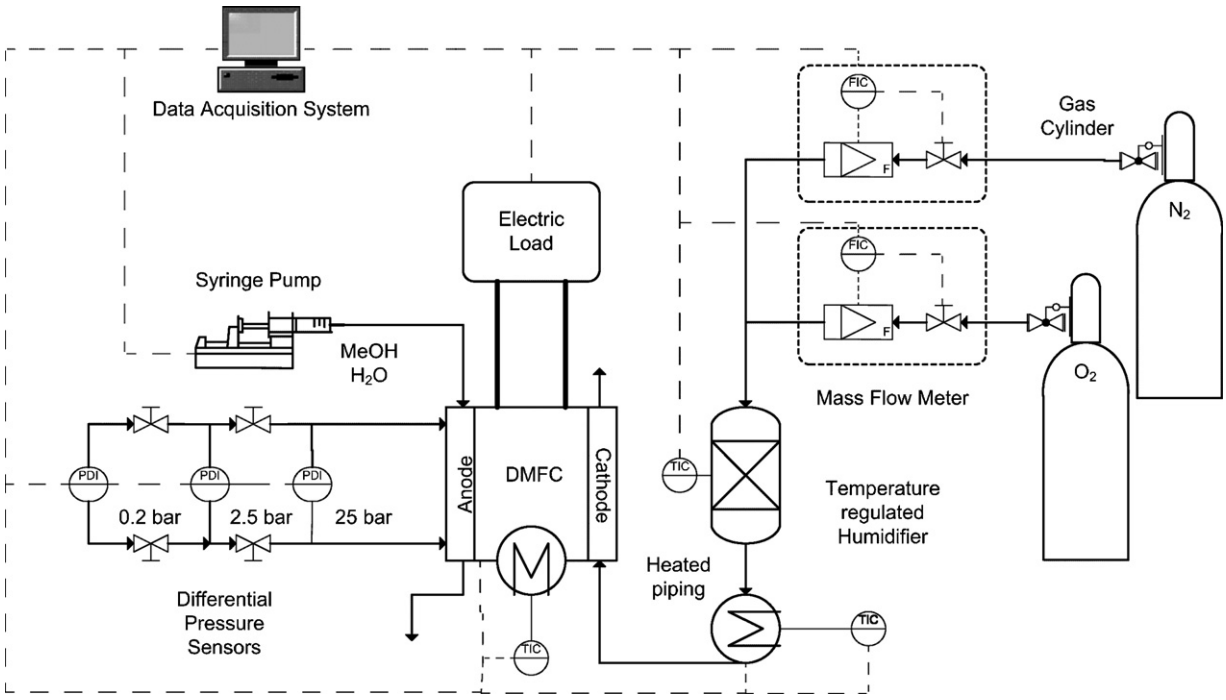

Fig. 4. Schematic diagram of the complete experimental setup.

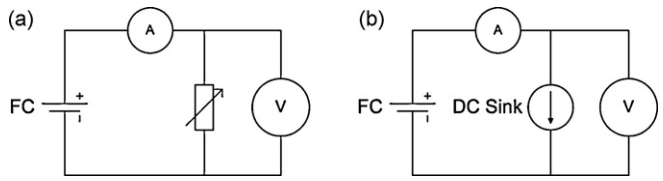

Fig. 5. Schematic diagrams of the electrical circuit of (a) the first measurement method: variable resistor as the electrical load (b) the second measurement method: galvanostatically–controlled current sink as the electrical load.

controllers (Bronkhorst, EL-Flow®) to a maximum gas volume flow rate V_g of 8 ml min^{-1}. The gas flow passes through a temperature-regulated humidifier, which nearly saturates the gas flow with humidity (RH = 95%, [21]). The subsequent tubing is heated with a careful temperature control (±0.5 °C) to prevent any condensation within.

The fuel cell assembly is provided with a controlled volume flow rate of a given methanol solution at the anode side and an adjusted and humidified gas flow rate at the cathode side, respectively. The temperature of the fuel cell assembly (FCA) is controlled by the heating block surrounding the FCA and a PT-1000 sensor attached in the vicinity of an electrode. The large heat capacity of the holder and of the heater guarantees a steady temperature within the FCA.

Preliminary tests have revealed that a serpentine flow field is advantageous for the cathode side in order to assure water removal of the MEA, which can block the O_2 supply to the MEA at a high power/current density. For the anode side two different flow field configurations have been tested; parallel and serpentine flow fields are assembled in a counter flow configuration.

2.3.2. Electrical measurement procedure

Two different techniques have been employed to measure the polarization curves of different parameter sets of the micro-direct methanol fuel cell.

As illustrated in Fig. 5a, the first measurement technique involves a variable resistor based on a N-channel discrete HEXFET® power MOSFET (metal-oxide semiconductor field effect transistor, IRF 1010N, International Rectifier Inc.) adjusting to a range from 11 mΩ to 10 MΩ directly controlled by LabView®. The resulting voltage is measured by an oscilloscope (LeCroy, waverunner LT224) and the current by a multimeter (Keithley 2000).

In the second measurement method the polarization curve is recorded galvanostatically, see Fig. 5b. The direct current source/sink (Keithley 6221) is operated in the second quadrant (positive current, negative voltage) incrementally controlling the range of set currents. The voltage is measured with a standard voltmeter (Keithley 2182A).

In the kinetic and ohmic regime of the fuel cell polarization curve, the differently measured polarization curves superimpose with in a relative error of 2%. In the third operating regime of a fuel cell the mass transfer limitation plays a dominant role. Hence, the different electrodynamics of the two measurement methods could in principle result in a deviation of the two polarization curves, but no significant such deviation was observed here. It can be stated that the influence of a voltage drop on the operating point on the variable resistor is resulting in a higher sensitivity to a disturbance.

2.3.3. Laser induced fluorescence microscopy

There exist several, non-intrusive methods for characterizing flow patterns in microchannels, such as brightfield microscopy, fluorescence microscopy and transient magnetic resonance imaging. In contrast to the commonly used brightfield microscopy, the here employed technique is fluorescence microscopy (LaVision Flow Master MITAS). The methanol solution is doped with 0.01 wt% Rhodamine 610 Chloride (Exciton), a fluorine dye inert to the chemical

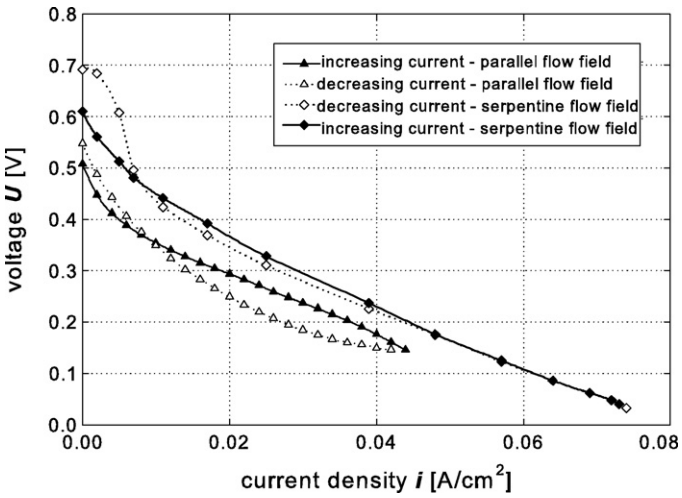

Fig. 6. Two sets of polarization curves measured with incrementally increasing/decreasing current densities for a parallel and a serpentine flow field configuration.

oxidation reaction of methanol occurring at the catalysts of the anode side. The dye, also known as Rhodamine B, fluoresce due to a laser excitation in a wavelength-shifted band resulting in flow images of well distinguishable phases; a clear contrast between the fluorescent liquid and the non-luminating gas phase is observable. Further details of the application of fluorescence microscopy in visualizing two-phase flow within microchannel networks simulating flow behavior of the anode side of a micro-DMFC can be found elsewhere [22].

3. Results and discussion

The polymer-based micro-DMFC is electrically characterized resulting in polarization curves. The prevailing strength of this measurement technique is based on the determination of the dependence of the investigated parameter on the electrical performance under a variable load. Therefore, a clear picture of the fuel cell or even stack performance can be projected to system relevant operating conditions.

In the following discussion an elaborate parameter study is presented starting with measurement implicit phenomena, continuing with the investigation of crucial parameters such as flow fields, temperature and volume flow rates and concluding with a demonstration of the fuel cell performance under bending conditions.

3.1. Hysteresis in polarisation curves

Fig. 6 shows a hysteresis of two polarisation curves with a difference of up to 0.05 V (or 10 mA cm^{-2}) resulting from the same set of parameters: SU-8 based parallel flow field on the anode side, a serpentine flow field on the cathode side, 0.56 ml min^{-1} volume flow rate of a 1 M methanol solution, 8 ml min^{-1} of a pure oxygen flow at the cathode side, cell temperature at 23 °C, galvanostatic measurement technique with a step size of 2 mA and a delay time of 10 s.

One curve is representing the results obtained by a current descending sequence, while the second plot is obtained from increasing the current with same discrete steps. The hysteresis effect is especially pronounced at higher currents allowing a similar argument as presented by [23]. They report three possible effects potentially causing a hysteresis of a polarization curve: (1) The accumulation of methanol, (2) CO_2 or (3) water at the reactive sites of the catalyst. Since we only can report the occurrence of the

hysteresis limited to the case of a serpentine flow field employed on the cathode side, it strongly supported by the optical observations in Section 3.5 that produced and expanding CO_2 bubbles start to cover active spots and hinder mass transport of methanol–water to the catalytic sites, hence, causing a performance hampering effect by reducing the effective/active fuel cell area.

During an incremental increase of the current density, the production rate of the CO_2 will proportionally increase but will lag behind the new potential. In the reverse/retracting scenario, incrementally decreasing the current density from a maximum, the already produced CO_2 gas bubbles still cover reaction sites and potentially even block the entire microchannel cross-sections, as seen in section 4.6.

This phenomenon is prone to parallel flow fields in which a cut-off of an entire channel segment is possible due to stagnant CO_2 bubbles. Under the assumption of sufficient pressure supply it is evident that the serpentine flow field will sweep through a possible blockage, therefore, showing this hysteresis to a much lesser extend, see Fig. 6.

3.2. Influence volume flow rates

3.2.1. Parallel flow field at the anode side

Fig. 7 displays a series of polarization curves investigating the effect of volume flow rates of the 1 M methanol solution in a parallel flow field at the anode side and a serpentine flow field at the cathode side at different temperature levels. Three volume flow rates are tested, 0.035, 0.14 and 0.56 ml min^{-1}, relating to the stoichiometries of 3.41, 13.65 and 54.61, respectively, at a reference operating current density of 100 mA cm^{-2}. The preheating temperature of the oxygen supply is set to the same temperature as the fuel cell block and the relative humidity at the cathode is kept constant.

At the ambient temperature of 23 °C, shown in Fig. 7a, the series of polarization curves is generally dominated by kinetic and ohmic losses except for the volume flow rate of 0.035 ml min^{-1} where a sudden drop of power density due to mass transfer limitation can be observed at 34 mA cm^{-2}. At a certain threshold value of the current density (proportional to the reaction conversion rate) the low volume flow rate is insufficient in removing the product gas CO_2 from the MEA surface depleting the active spots at the three-phase boundary from methanol and water and, therefore, causing a collapse of the power density.

The increase of volume flow rate from 0.035 to 0.14 ml min^{-1} results in a stabilization of the power density and current density plot resulting in a maximum power density of 5.35 mW cm^{-2} at 36 mA cm^{-2}. A further increase of volume flow rate to 0.56 ml min^{-1} yields in contradiction to theory a lower current density and therefore a lower power density. In the literature [7] it has been reported that an increase of volume flow rate does not necessarily mean an increase of power density. After some initial improvements, the power/current density curve is unaffected by any further volume flow rate increase due the limitation of the reaction rate. However, the slight decrease of performance resulting in a steeper slope of the current density curve indicates an increase of the inner resistance. Therefore, the fact of a certain misalignment of the two opposing flow fields should not be underestimated since this can lead, especially at higher volume flow rates, to a stronger deflection of the MEA resulting in an increase of the intrinsic/inner resistance of the fuel cell assembly.

Further, an increase of the volume low rate of the methanol solution on the anode side, while leaving the oxygen supply constant, is shifting the ratio between the two stoichiometries, see Table 1. According to Kulikosky [24] this outbalanced stoichiometry of the methanol solution causes the fuel cell to operate locally as an

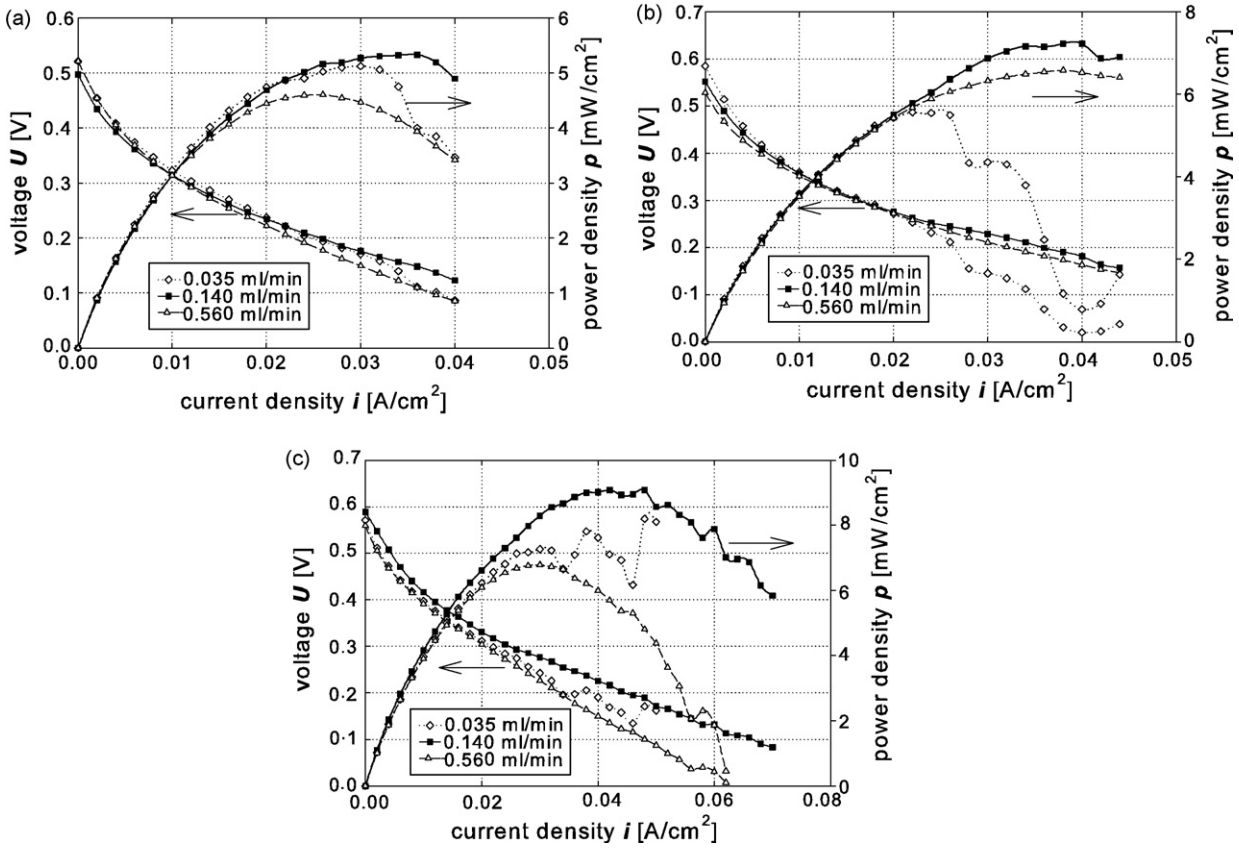

Fig. 7. Polarization curves of the parallel flow field in dependence of the volume flow rate at different temperature levels: (a) $T = 23$, (b) $T = 40$, and (c) $T = 60$ °C.

Table 1
Stoichiometry ratios calculated for a reference current density of 100 mA cm^{-2} at different volume flow rates on the anode side for a constant O_2 volume flow rate of 8 ml min^{-1}.

$\dot{V}_{CH_3OH}$ [ml min^{-1}]	0.035	0.140	0.560
λ_{CH_3OH}	3.41	13.65	54.61
$\lambda_{O_2}/\lambda_{CH_3OH}$	6.17	1.54	0.385

electrolytic cell (performing inner reforming), therefore, reducing the overall performance of the fuel cell.

In Fig. 7b and c the temperature level is elevated to 40 and 60 °C, respectively. The recorded current and power density curves are of similar nature as discussed for Fig. 7a. The predominance of the kinetic and the ohmic effect are the prevailing features of the shape of the current density curve. Due to the higher temperature level, the effects seen in Fig. 7a are more pronounced and the power maximum is shifted to 7.22 mW cm^{-2} at 40 mA cm^{-2} for 40 °C and to 9.08 mW cm^{-2} at 48 mA cm^{-2} for 60 °C at 0.14 ml min^{-1}.

The mass transfer limitation plays a more dominant role at higher temperatures, as can be seen from Fig. 7b and c by the drastic drop of the power density. At 40 °C this effect sets in at 26 mA cm^{-2}, earlier than at 23 °C. In Fig. 7c at 60 °C the curve displays not a distinct drop, but an unsteady behavior beyond 32 mA cm^{-2} which results from CO_2 gas bubbles irregularly departing from the MEA occasionally blocking entire channel segments.

3.2.2. Serpentine flow field at the anode side

Fig. 8 shows the effect of the volume flow rate at different temperature levels under the application of a serpentine flow field at the anode side and a serpentine flow field at the cathode side. The current density curves measured by the variable resistor with a time delay of 30 s exhibit kinetic and ohmic control and no mass transfer limitation is apparent. The maximum power densities are 8.87 mW cm^{-2} at 23 °C, 12.3 mW cm^{-2} at 40 °C and 19.0 mW cm^{-2} at 60 °C at a 1 M methanol solution volume flow rate of 0.14 ml min^{-1}, therefore, exceeding the maximum power output of the parallel flow field assembly shown in Fig. 7 by a factor of 2.

Despite the fact that at a given volume flow rate the serpentine flow field yields a much higher pressure drop necessitating a higher pumping power the homogeneous reactant supply and the product gas removal is ensured across the whole active area of the MEA. This also points toward the limitations and applicability range of numerical studies such as [25] modeling innovative geometry concepts, but neglecting for simplicity the effect of two-phase flow phenomena.

It is interesting to note that the volume flow rate dependence of the power output is much less pronounced than for the parallel channels. The general trend seen in Fig. 8a is a slight increase in power density and a higher maximum current density by an increased volume flow rate.

At 40 °C, in Fig. 8b, at a volume flow rate of 0.035 ml min^{-1} the influence of an unsteady two-phase flow on the polarization curve, hence the power density curve is apparent. At 60 °C, in Fig. 8c, at a volume flow rate of 0.017 ml min^{-1} mass transfer limitation plays a dominant role starting from 68 mA cm^{-2}. In order to prevail an unsteady fuel cell performance, the experiments suggest to surpass a certain flow rate; for this specific fuel cell assembly 0.14 ml min^{-1} of a 1 M methanol solution proves to be ideal.

Another important finding is the higher open-current potential for the serpentine flow field. It is interesting that a simple change in

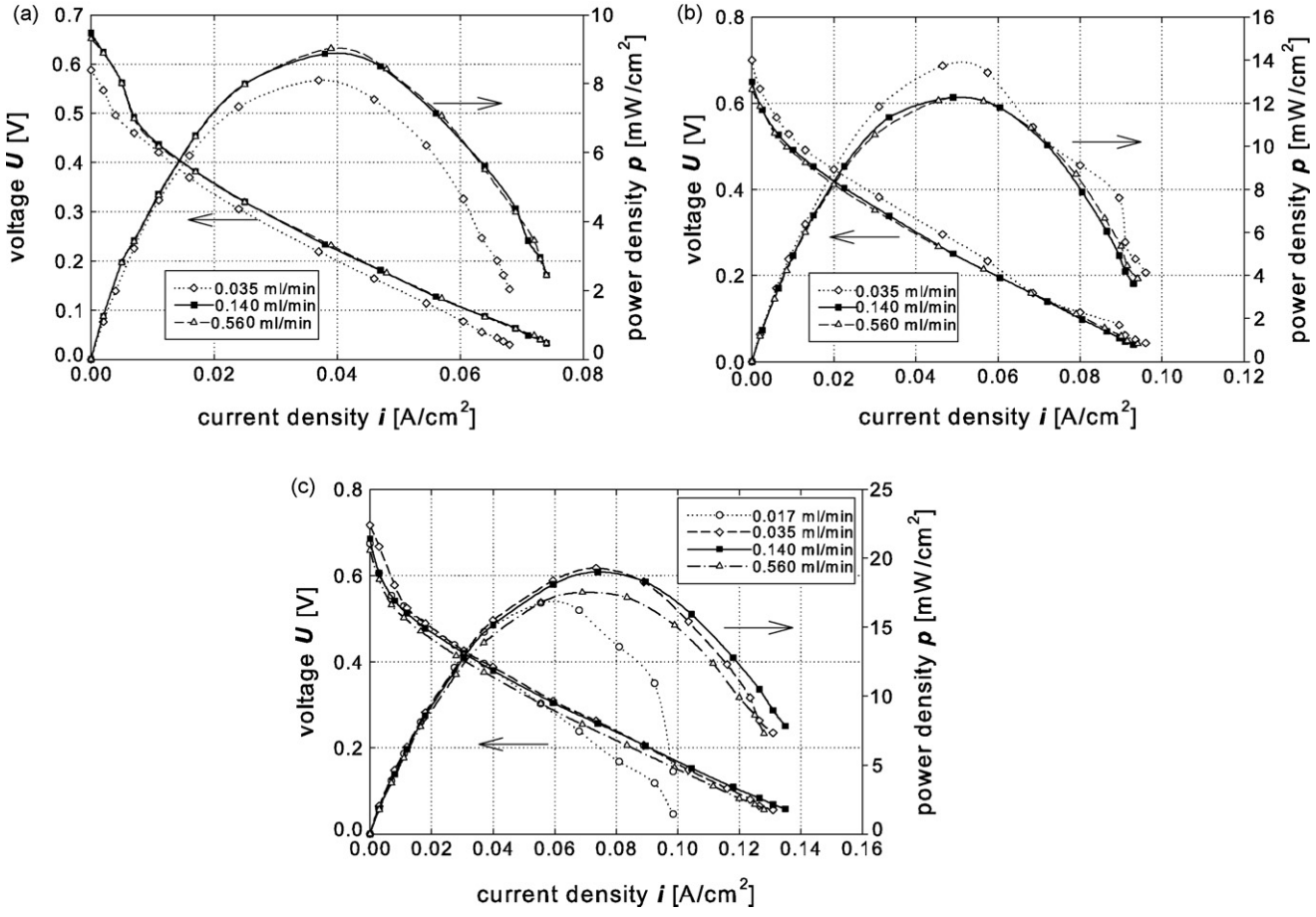

Fig. 8. Polarization curves of the serpentine flow field in dependence of the volume flow rate at different temperature levels: (a) T = 23, (b) T = 40, and (c) T = 60 °C.

flow field geometry inscribed as a channel network in the electrode can influence the open-current potential, which is dependent on namely two factors: the methanol crossover through the MEA and the internal current. Since the MEA is not changed, the internal current is not altered as well, proving the influence of the flow field on the methanol crossover by altering the local pressure distribution and therefore affecting the osmotic drag of methanol.

3.3. Influence of temperature

3.3.1. Parallel flow field at the anode side

Temperature is an essential parameter for the operation of a fuel cell additionally shown in Fig. 7 at different volume flow rates. The experiments were performed with the same set of parameters: on the anode side a parallel flow field, 1 M methanol concentration, cathode side serpentine flow field and an O_2 gas flow rate of 8 ml min^{-1}, employment of the galvanostatic measurement technique with a step size of 2 mA and a delay time between the measurement points of 10 s.

In Fig. 7, comparing different temperatures at a volume flow rate of 0.035 ml min^{-1} the fuel cell shows an unsteady behavior at the power densities above 26 mA cm^{-2} resulting from the strong influence of bubble generation and blocking of channel segments on the anode side. The volume flow rate distributed across 25 parallel channels is strongly reducing the effective volume flow rate per parallel channel, therefore exposing it to flow abnormalities.

As the comparison of volume flow rates in the last section has shown, the power maxima are reached at 0.14 ml min^{-1} flow rates. Increasing the temperature from ambient 23–40 and 60 °C is lifting the power density from 5.35 to 7.22 mW cm^{-2} and to 9.08 mW cm^{-2} and the open-current potential to 0.497, 0.552 and 0.588 V, respectively. The polarization curves are depicting an evident kinetic and ohmic influence, but no mass transfer limitation within the measured regime. However, at high volume flow rates mass transfer limitation is displayed above 56 mA cm^{-2} at a temperature of 60 °C, see Fig. 7.

3.3.2. Serpentine flow field at the anode side

The clear dependence of the fuel cell performance on the temperature seen above for parallel flow fields, holds also for serpentine flow fields. The effect of temperature is also investigated in Fig. 8 over a series of 1M methanol solution flow rates: 0.035, 0.07, 0.14, 0.56 ml min^{-1}. Furthermore, the experiments were performed with the same set of parameters: on the anode side a parallel flow field, 1 M methanol concentration, cathode side serpentine flow field and an O_2 gas flow rate of 8 ml min^{-1}, employment of the variable resistor measurement technique with a delay time between the measurement points of 30 s.

All curves plotted show a clear dependence on kinetic and ohmic limitations with the exception at low volume flow rates, where mass transfer limitations can be observed at 23 °C and at 40 °C starting from 60 mA cm^{-2}.

It can be stated as a general observation that temperature has a strong reaction enhancing effect on the performance of a polymer film based micro-DMFC. As seen in Fig. 8, the presented fuel cell in this paper already has at a reasonably low volume flow rate of 0.07 ml min^{-1} of a 1 M methanol solution a good electrical performance of 8.49 mW cm^{-2} at 38 mA cm^{-2} at ambient conditions of 23 °C, which can be compared to a standard start-up scenario for a fuel cell system.

Increased operating temperatures to 40 °C, 60 °C and even a maximum temperature of 88 °C strongly improve the electrical performance of the fuel cell yielding maximum power densities of 12.7 mW cm^{-2} at 46 mA cm^{-2}, 19.3 mW cm^{-2} at 74 mA cm^{-2}, 21.7 mW cm^{-2} at 86 mA cm^{-2}, respectively.

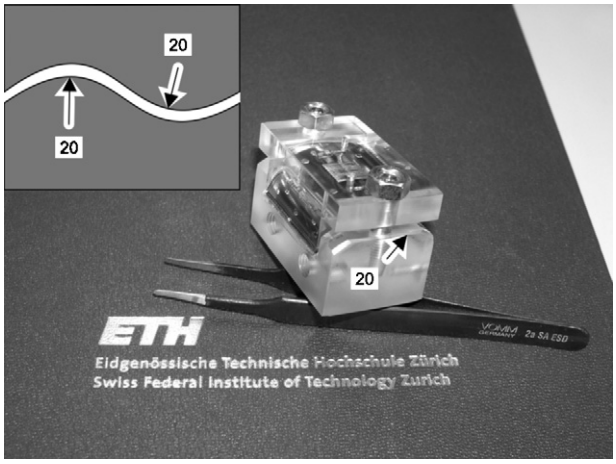

Fig. 9. Picture of the PMMA holder for the bending experiments and a schematical cross-section of the "S-shaped" profile.

In comparison to the earlier employed parallel flow field, an averagely increased open-current potential of +10 mV, considerably higher power densities of up to 22 mW cm^{-2} and noticeably larger current densities of up to 150 mA cm^{-2} can be observed.

3.4. Fuel cell performance under bending

A further study was performed focusing on the electrical characterization of the fuel cell performance under bending to demonstrate the feasibility of the fuel cell under flexed operating conditions with the following parameters: on the anode side a parallel flow field and volume flow rate of 0.14 ml min^{-1} of a 1 M methanol solution, on the cathode side a serpentine flow field and an O_2 gas flow rate of 8 ml min^{-1}, employment of the galvanostatic measurement technique with a step size of 2 mA and a delay time between the measurement point of 10 s at an ambient temperature of 23 °C. Three different scenarios have been chosen: (I) no bending, planar use of the fuel cell, (II) bending with a constant curvature of 20 mm at the cathode side, and (III) "S-shaped" bending with two opposing radii of 20 mm. The curvature is achieved by inserting the fuel cell assembly into an accordingly shaped holder, Fig. 9.

Fig. 10 shows the polarization curves of the three mentioned scenarios. The curves depict only a slight divergence from each other. The strongest deviation of the case (II) from (I) can be explained by the inhomogeneous contact pressure resulting in a reduced inner

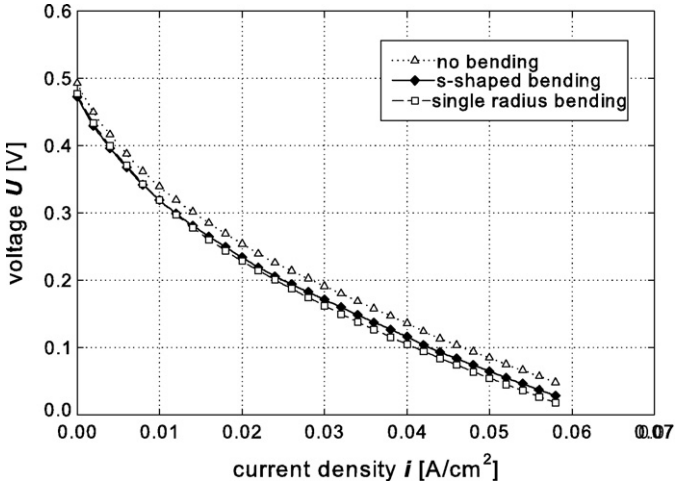

Fig. 10. Influence of the bending on the electrical performance for cases (I), (II), (III).

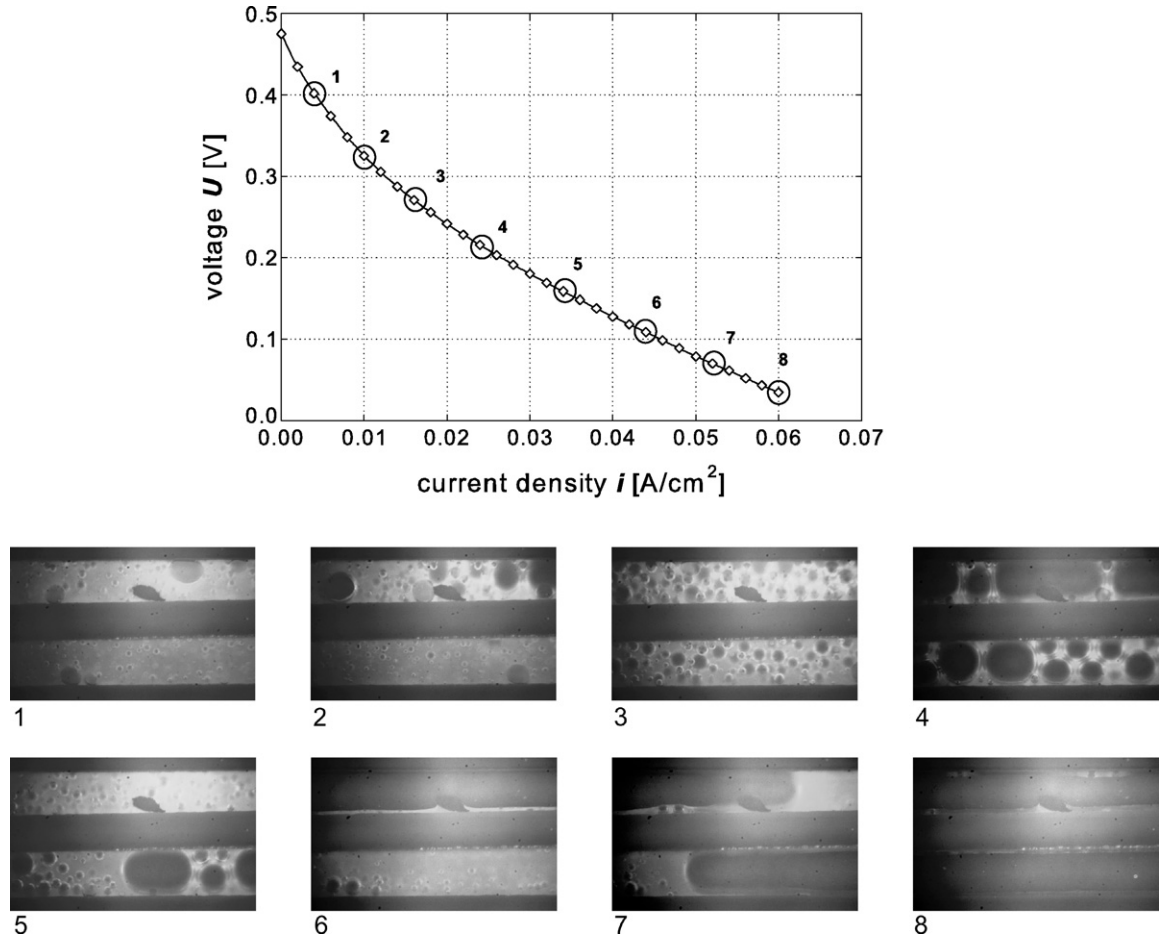

Fig. 11. LIF-visualization of two-phase flow in serpentine channel segments correlated to the according current density.

resistance of the assembly. Furthermore, the increase of the inner resistance can be due to micro-fractures in the metallization layer of the polymer in case (II) and (III). Case (III) minimally deviates from case (II); similar aspects as for case (II) have to be taken into consideration.

The major finding of this study revealed the feasibility in principle of the employment of the demonstrated fuel cell assembly for bent or flexed applications in a variety of devices without a marked deviation in performance.

3.5. Micro-LIF: two-phase flow in correlation to the polarization curves

Fig. 11 shows a flow-visualization performed with fluorescence microscopy of the two-phase flow occurring at the anode side due to the oxidation of methanol producing gas CO_2. Details of the measurement procedure are presented in [22].

The experimental series is performed with the following parameters: on the anode side a parallel flow field and volume flow rate of 0.14 ml min^{-1} of a 1 M methanol solution, on the cathode side a serpentine flow field and an O_2 gas flow rate of 8 ml min^{-1}, employment of the galvanostatic measurement technique with a step size of 2 mA and a delay time between the measurement point of 10 s at an ambient temperature of 23 °C.

The images of the visualized two-phase flow are linked to the corresponding current density on the polarization curve. It can be observed that the gas bubble size and, therefore, the gas/liquid volume ratio inside the microchannel are steadily increasing from (1) to (3) proportional to the corresponding current density. At (4) the size of the gas bubbles is reaching the diameter of the microchannel, hence forming elongated bubbles and accordingly flow regimes as described and studied in two-phase microfluidics [22,26]. With a further increase in current density at a given volume flow rate the product gas starts occupying entire segments of the microchannel with only a thin liquid film of 1 M methanol solution remaining on the channel walls. It is evident that the global volume flow rate of the 1 M methanol solution is strongly reduced at a local scale depleting the regional active sites of reactants; hence a drop in local current density after (8) can be expected.

The flow-visualization illustrates the strong effect of CO_2 gas generation on the fluid flow inside the flow field and the strong influence on the homogeneous reactant supply to the MEA.

4. Conclusions

The focus of this study was the demonstration and the electrical characterization of a flexible, thin film polymer-based direct methanol micro-fuel cell. In the preamble of this paper the concept for the fabrication of a FDMMFC is presented. While employing a standard MEA consisting of a Nafion®-117 membrane coated with Pt-black on the cathode side and Pt/Ru on the anode side without a gas diffusion layer, the electrodes are fabricated on 200 μm thick SU-8, photosensitive polymer film showing the degree of flexibility. A subsequent physical vapor deposition of a Cr/Au bilayer on the photolithographic microstructured polymer functionalizes the thin film to a conducting electrode.

During the course of the paper, several performance-influencing parameters were investigated. In a first step the pervasively

occurring hysteresis in the polarization curves of descending and thereafter rising current densities is discussed. It was found that the hysteresis is especially pronounced in parallel flow field fuel cells at the anode, indicating the influence of fluid dynamical aspects as CO_2 stagnation on reactive sites.

In a parallel flow field at the anode and a serpentine flow field at the cathode side the variation of the volume flow rate has yielded an optimum at 0.14 ml min^{-1} of a 1 M methanol solution in a 200 μm × 200 μm microchannel for an active fuel cell area of 10 mm × 10 mm. For a serpentine flow field at the anode side an increase in volume flow rate at the anode side at a constant O_2 gas flow rate of 8 ml min^{-1} at the cathode side achieves a consequently higher electrical performance.

The effect of temperature for both kinds of flow fields resulted in a generally improved power density. A maximum power density of 21.7 mW cm^{-2} was achieved at 86 mA cm^{-2} mA at the highest temperature level of 88 °C.

In direct comparison of the two different flow fields at the anode, the serpentine flow field showed an average increased open-current potential of +10 mV, considerably higher power densities of up to 22 mW cm^{-2} and noticeably larger current densities of up to 150 mA cm^{-2} than for the parallel flow field.

We also demonstrated the feasibility of the fuel cell operation under bending with a curvature of 20 mm. The current density did not show any significant decrease. However, a slight drop can be observed due to the effect of inhomogeneous contact resistance and possibly micro-fractures in the conducting metal top layer. A "S-shaped" bending did not show any significant further aspects, either.

In comparison to the rigid substrate based micro-fuel cells from the literature [7,12] the herein presented DMFC concept still proofed to achieve reasonably high power densities of up to 20 mW cm^{-2} even under bending conditions.

The paper is concluded with a flow-visualization in the microchannels at the anode side demonstrating the strong impact of CO_2 bubble generation on the reactant supply to the MEA and along the remainder of the channel network.

Even though several effects and parameters have been investigated for this novel concept of a flexible direct methanol micro-fuel cell, further experiments are needed especially in quantifying the influence of two-phase fluid dynamics on the active sites of the reaction and therefore on the local current density distribution.

References

[1] B.Y. Park, M.J. Madou, Journal of Power Sources 162 (2006) 369–379.
[2] M. Lundstrom, Science 299 (2003) 210–211.
[3] M. Salomon, Lithium Batteries: Present Trends and Prospects, Army Research Laboratory, Fort Monmouth, NJ, 1996.
[4] C. Stone, Fuel Cells Bulletin (2007) 12–15.
[5] R. Hahn, S. Wagner, A. Schmitz, H. Reichl, Journal of Power Sources 131 (2004) 73–78.
[6] G.Q. Lu, C.Y. Wang, Journal of Power Sources 134 (2004) 33–40.
[7] G.Q. Lu, C.Y. Wang, T.J. Yen, X. Zhang, Electrochimica Acta 49 (2004) 821–828.
[8] T.A. Trabold, Heat Transfer Engineering 26 (2005) 3–12.
[9] H.Y. Cha, H.G. Choi, J.D. Nam, Y. Lee, S.M. Cho, E.S. Lee, J.K. Lee, C.H. Chung, Electrochimica Acta 50 (2004) 795–799.
[10] S.K. Kamarudin, W.R.W. Daud, S.L. Ho, U.A. Hasran, Journal of Power Sources 163 (2007) 743–754.
[11] A. Kundu, J.H. Jang, J.H. Gil, C.R. Jung, H.R. Lee, S.H. Kim, B. Ku, Y.S. Oh, Journal of Power Sources 170 (2007) 67–78.
[12] S.C. Kelley, G.A. Deluga, W.H. Smyrl, Electrochemical and Solid State Letters 3 (2000) 407–409.
[13] G.T.A. Kovacs, C.W. Storment, M. Halksmiller, C.R. Belczynski, C.C. Dellasantina, E.R. Lewis, N.I. Maluf, IEEE Transactions on Biomedical Engineering 41 (1994) 567–577.
[14] B.Y. Ahn, E.B. Duoss, M.J. Motala, X.Y. Guo, S.I. Park, Y.J. Xiong, J. Yoon, R.G. Nuzzo, J.A. Rogers, J.A. Lewis, Science 323 (2009) 1590–1593.
[15] G. Dennler, S. Bereznev, D. Fichou, K. Holl, D. Ilic, R. Koeppe, M. Krebs, A. Labouret, C. Lungenschmied, A. Marchenko, D. Meissner, E. Mellikov, J. Meot, A. Meyer, T. Meyer, H. Neugebauer, A. Opik, N.S. Sariciftci, S. Taillemite, T. Wohrle, Solar Energy 81 (2007) 947–957.
[16] B.D. Gates, Science 323 (2009) 1566–1567.
[17] M.J. Madou, Fundamentals of Microfabrication, 2nd ed., CRC Press, Boca Raton/London/New York/Washington, DC, 2001.
[18] Y.N. Xia, G.M. Whitesides, Annual Review of Materials Science 28 (1998) 153–184.
[19] C.W. Wong, T.S. Zhao, Q. Ye, J.G. Liu, Journal of the Electrochemical Society 152 (2005) A1600–A1605.
[20] K. Scott, W.M. Taama, P. Argyropoulos, K. Sundmacher, Journal of Power Sources 83 (1999) 204–216.
[21] N. Koc, Master Masterthesis, D-MAVT, ETH Zurich, Zurich, 2008.
[22] C. Weinmueller, N. Hotz, A. Mueller, D. Poulikakos, International Journal of Multiphase Flow 35 (2009) 760–772.
[23] A. Casalegno, R. Marchesi, Journal of Power Sources 175 (2008) 372–382.
[24] A.A. Kulikovsky, Electrochemistry Communications 10 (2008) 1415–1418.
[25] S.M. Senn, D. Poulikakos, International Journal of Heat and Mass Transfer 49 (2006) 1516–1528.
[26] T. Cubaud, C.M. Ho, Physics of Fluids 16 (2004) 4575–4585.